THE JOURNAL OF PHYSICAL CHEMISTRY B

Article

pubs.acs.org/JPCB

Exciton Self Trapping in Photosynthetic Pigment–Protein Complexes Studied by Single-Molecule Spectroscopy

Ralf Kunz,[†] Kõu Timpmann,[‡] June Southall,[§] Richard J. Cogdell,[§] Arvi Freiberg,[‡,∥] and Jürgen Köhler*[,†]

[†]Experimental Physics IV and Bayreuth Institute for Macromolecular Research (BIMF), University of Bayreuth, 95440 Bayreuth, Germany

[‡]Institute of Physics, University of Tartu, Riia 142, Tartu EE-51014, Estonia

[§]Institute of Molecular, Cell and Systems Biology, College of Medical Veterinary and Life Sciences, Biomedical Research Building, University of Glasgow, Glasgow G12 8QQ, Scotland, United Kingdom

[∥]Institute of Molecular and Cell Biology, University of Tartu, Riia 23, Tartu EE-51010, Estonia

ABSTRACT: Evidence for the formation of self-trapped exciton states in photosynthetic antenna complexes is provided by comparing single-molecule fluorescence–excitation and emission spectra that have been recorded from the same individual LH2 complex from *Rhodopseudomonas acidophila*. While the excitation spectra showed the signatures for the B800 and B850 bands as observed previously, two distinctively different types of emission spectra were found. One group of antenna complexes shows spectra with a relatively narrow spectral profile with a clear signature of a zero-phonon line, whereas the other group of complexes displays spectra that consist only of a broad featureless band. Analysis of these data reveals clear correlations between the spectral position of the emission, the width of the spectral profile, and the associated electron–phonon coupling strength.

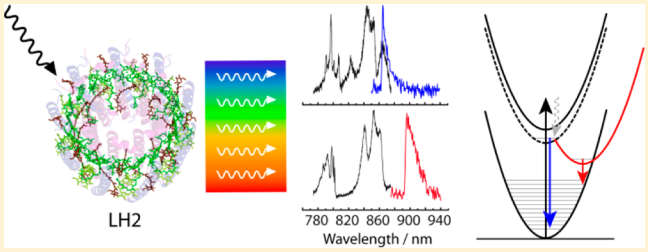

INTRODUCTION

Purple photosynthetic bacteria have evolved an elegant system of modular units that make up their light-harvesting apparatus. These modules consist of pairs of hydrophobic, low molecular weight polypeptides, called α and β (usually 50–60 amino acids long), that noncovalently bind a small number of bacteriochlorophyll (BChl *a*) and carotenoid (Car) molecules. The modules then oligomerize to produce the functional light-harvesting complexes.[1−6] Light-harvesting complex 1 (LH1) encloses the reaction center (RC) and forms the core complex, whereas the peripheral light-harvesting complexes (LH2) are arranged around the perimeter of the RC-LH1 complex in a two-dimensional array.

Significant progress in our understanding of the light-harvesting reactions of photosynthesis was achieved when the structure of the LH2 pigment–protein complex from the purple bacterium *Rhodopseudomonas (Rps.) acidophila* was resolved.[1] This complex accommodates 27 BChl *a* molecules and 9 carotenoids. The BChl *a* molecules are organized in two concentric rings referred to as B800 and B850, according to the spectral position of their room temperature absorption bands. From the intermolecular distances determined by the X-ray structure, it can be concluded that the dipolar interaction between neighboring BChl *a* molecules in the B850 ring is significant and leads to delocalized excited states that are coherently distributed at least over a part of the ring. Hence a natural starting point to describe the lowest electronically excited states of this assembly is based on the Frenkel exciton formalism.[7−9] Neglecting the slight dimerization of the B850 BChl *a* molecules, the proper eigenstates are exciton states and are characterized by a quantum number, *k*, which can take the values 0, ±1, ±2, ..., ±8, and 9. Due to the circular symmetry, only the states $k = \pm 1$ carry an appreciable transition-dipole moment that makes them accessible for optical spectroscopy. Structural and/or energetic heterogeneities are usually accounted for by random and/or correlated disorder in the site energies of and in the couplings between the BChl *a* molecules. The main effects of disorder on the exciton manifold are a mixing of the different exciton levels, a modification of the energy separation of the exciton levels and lifting their pairwise degeneracy, and a redistribution of oscillator strength to nearby states.[10,11] Overcoming the problem of sample heterogeneity and ensemble averaging by exploiting single-molecule techniques at low temperatures has helped to further refine the theoretical description of the B850 excitations.[12−18] The "disordered Frenkel exciton" model grasps the essential features observed in absorption and fluorescence–excitation spectroscopy for these systems.

However, comparison of ensemble-absorption and emission spectra from LH2 complexes has led to several discrepancies that are inconsistent with the disordered Frenkel exciton approach:[19,20] (i) Simulations based on the exciton model

Received: April 26, 2012
Revised: June 13, 2012
Published: August 21, 2012

   dx.doi.org/10.1021/jp3040456 | *J. Phys. Chem. B* 2012, 116, 11017–11023

distribute the lowest exciton state over a range of 140 cm^{-1} (fwhm) on the low energy side of the ensemble absorption spectrum. This number is in agreement with results from hole-burning and single-molecule experiments.[13,21−23] Yet, the width of the respective ensemble emission spectrum exceeds this figure by more than a factor of 2.[20,24] (ii) Experimental evidence has been found that the emission spectrum is essentially homogeneously broadened suggesting that exciton−phonon coupling for the transition from the relaxed excited state must be strong.[19] This is in contrast to the quasiline absorption spectrum, which is mostly inhomogeneously broadened. Similar inconsistencies have been found for LH1 as well.[25−28] (iii) Raising the temperature should thermally populate the strongly allowed $k = \pm 1$ exciton states and result in a significant reduction of the fluorescence lifetime. However, the fluorescence lifetime changes only by about 20% between cryogenic temperatures and room temperature.[20] On the basis of the exciton model this can only be explained by assuming static disorder in the site energies of the individual BChl a pigments that is much too large to be consistent with the absorption spectrum. (iv) While single-molecule fluorescence−excitation spectra are consistent with the disordered Frenkel exciton model, implying the observation of (fully) delocalized excitons,[12,14,15,17,18,29,30] time-resolved spectroscopy has led to the conclusion that the excitation energy is localized on about 2−7 pigments.[20,31−34]

In order trying to explain these conflicting observations, the Freiberg group has put forward a model that involves exciton self-trapping in the B850 assembly.[19,20,28,35] Self-trapping of excitons is a well-known phenomenon in solids.[36−40] It refers to the fact that, due to exciton−phonon interaction, the exciton induces a structural reorganization of its environment, which lowers its energy to an extent such that the excitation energy gets trapped on a limited region of the aggregate. This phenomenon is also referred to as polaron formation. It has been shown theoretically that in one-dimensional systems self-trapping inherently takes place for any nonvanishing electron−phonon coupling.[37] Within certain reservations, the B850 ring, consisting of strongly electronically coupled BChl *a* molecules, can be considered as a one-dimensional system. Freiberg and co-workers have developed a consistent description of the experimental findings based on ensemble studies on LH2 complexes.[20,41−43] However, the great difficulty encountered in these biological systems is the large heterogeneity of the samples that smears out the subtle details in the ensemble-averaged spectra. In order to avoid ensemble-averaging and to try to find direct evidence for self-trapping of excitons in the B850 manifold of LH2, it would be desirable to perform fluorescence−excitation and fluorescence emission spectroscopy on the same individual complex. Previous single-molecule studies that recorded emission spectra from these systems did not focus on possible self-trapping processes and/or were conducted at room temperatures where important spectral details are masked by thermal broadening.[44−51] The advantages of working at low temperatures are negligible photobleaching, which enables long observation times and concomitantly an improvement of the signal-to-noise ratio of the spectra, as well as a reduction in the linewidths of the spectral features due to the suppression of (thermal) motions of the nuclei. This allows us to resolve narrow spectral features which, even for a single molecule, would be hopelessly broadened at room temperature. Since electrons are very light particles, processes that involve their movements, i.e., transitions into electronically excited states, are at low temperature as active as at room temperature. In other words cryogenic conditions are well suited to obtain a good approximation of the electronic structure of biomolecules. This should not be confused with dynamical properties of proteins, i.e., those that involve molecular rearrangements. The rates of such relaxations, of course, depend on temperature and do not agree with the corresponding rates under physiological conditions.[52] However, working at cryogenic temperatures shifts the time scale for these fluctuations into a range that is experimentally accessible.

Here we report on low-temperature fluorescence−excitation and emission spectroscopy carried out on the same individual LH2 complex that allows for a direct comparison of the absorbing and emitting electronic states. Analysis of the spectral profiles obtained leads us to conclude that for some of the LH2 complexes emitting at the red end of the spectrum exciton self-trapping does indeed occur.

EXPERIMENTAL SECTION

Sample Preparation. The LH2 complexes from the species *Rps. acidophila* (strain 10050) were isolated and purified as described previously.[53] After purification, the LH2 complexes were transferred to a buffer solution (20 mM Tris HCl, pH 8.0, 0.1% LDAO) and stored in small aliquots at −80 °C until used. This stock solution was diluted in detergent buffer solution in several steps to a concentration of about 10^{-11} M. In the last dilution step also 1.8% (w/w) polyvinyl alcohol (PVA; M_w = 125 000 g/mol) was present. A drop (20 μL) of this solution was spin-coated on a cleaned quartz (SiO_2) substrate by spinning it for 10 s at 500 rpm and 60 s at 2500 rpm, producing high quality amorphous polymer films with a thickness of about 100 nm in which the pigment−protein complexes are embedded. The samples were immediately mounted in a liquid-helium cryostat and cooled to 1.2 K. For studying ensembles of LH2 complexes the stock solution was diluted to 10^{-6} M, and further the same protocol as described above was followed.

Optical Setup. For the optical experiments the samples were illuminated with a continuous-wave tunable titanium-sapphire (Ti:Sa) laser (3900S, Spectra Physics) pumped by a frequency doubled continuous-wave neodymium−yttrium−vanadate (Nd:YVO_4) laser (Millennia Vs, Spectra Physics) using a home build microscope that can be operated either in widefield or confocal mode. To obtain a well-defined variation of the wavelength of the Ti:Sa laser the intracavity birefringent filter has been rotated with a motorized micrometer screw. For calibration purposes a wavemeter (WaveMaster, Coherent) has been used and an accuracy as well as a reproducibility of 1 cm^{-1} for the laser frequency has been verified.

First a 40 × 40 μm^2 wide-field image of the sample was taken by exciting the sample around 855 nm through a band-pass (BP) excitation filter (BP 858/30; Dr. Hugo Anders). The emission from the sample was collected by a microscope objective (Mikrothek, NA = 0.85) that was mounted inside the cryostat and the signal was focused onto a back-illuminated CCD camera (512 SB, Princeton Instruments) after passing band-pass filters (BP 900/50; AHF Analysetechnik) that block residual laser light. Next, a spatially well-isolated complex was selected from the wide-field image, and the microscope was switched to the confocal mode. In this mode the excitation volume is in the order of 0.1 μm^3. A well-controlled adjustment of this volume with respect to the sample is achieved by a pair of telecentric lenses.

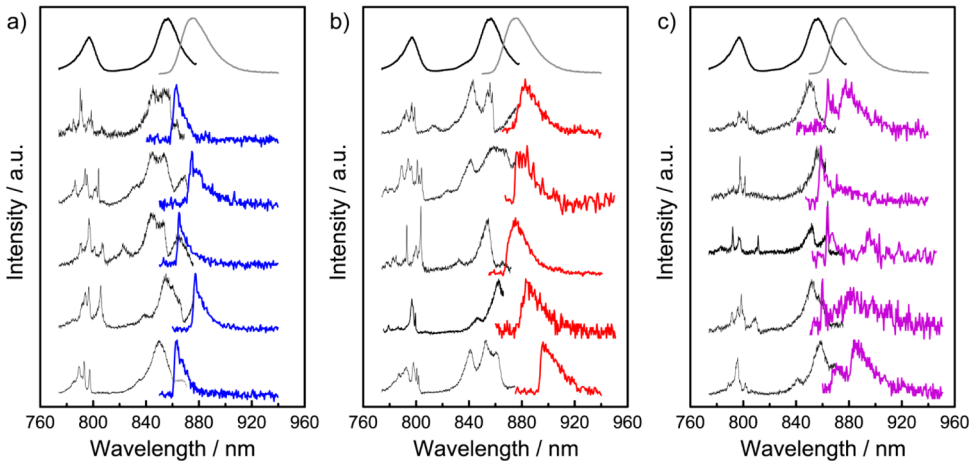

Figure 1. Fluorescence−excitation (black lines) and emission spectra (colored lines) from LH2 complexes of *Rps. acidophila*. In each panel the top traces show the ensemble spectra for comparison and five examples of excitation/emission spectra recorded from the same individual complex. The spectra are normalized to their peak intensity (of the B850 band for fluorescence−excitation) and offset for clarity. The fluorescence−excitation spectra correspond to averages over all polarizations of the excitation light, and the excitation power was 100 W/cm^2. The emission spectra were detected above 830 nm and the excitation power was 1 kW/cm^2. The exposure times were 60 s. All spectra were measured at 1.2 K. (a) Type I: Complexes with narrow, sharp edged emission spectrum. (b) Type II: Complexes with broad, featureless emission spectra. (c) Type III: Complexes for which the emission spectra show features from both previous categories.

Fluorescence−Excitation Spectroscopy. Fluorescence−excitation spectra have been recorded by scanning the linearly polarized excitation light either from 774 to 872 nm or from 774 to 876 nm with a scanning rate of 3 nm/s (~50 cm^{-1}/s). The excitation intensity was about 100 W/cm^2. The polarization of the excitation light was rotated in steps of 6.4° between two successive scans by means of a waveplate. The emission passed through a set of bandpass filters (BP900/50, BP890/20; AHF Analysetechnik, BP893/21; Dr. Hugo Anders) and was focused onto a single-photon counting avalanche photodiode (APD) (SPCM-AQR-16, EG&G). The fluorescence−excitation spectra shown in this study correspond to the averages over all polarizations of the excitation light. All fluorescence−excitation spectra have been corrected for variations of the laser intensity as a function of the wavelength.

Fluorescence-emission spectroscopy. For the emission spectroscopy the individual complexes were excited around 800 nm through a band-pass filter (BP805/60; AHF Analysetechnik). Since the absorption bands in this spectral range are rather narrow the laser wavelength was wobbled with an amplitude of about 5 nm at a rate of 3 nm/s around the B800 absorptions of the complex under study. The polarization of the excitation light was rotated as described above. By changing the detection path of the setup using a flip mirror, the emitted light could be directed through a set of dielectric long-pass filters (LP830; AHF Analysetechnik) and was dispersed in a spectrometer (SpectraPro-150, 300 lines/mm, Acton Research Corporation) providing a spectral resolution of 1.5 nm (20 cm^{-1}). The signal was detected with a CCD camera (iDus DV420A-OE, Andor Technology or Luca-R 604M-OM, Andor Technology) using an exposure time of 60 s (iDus) or 600 s (Luca), respectively. The sensitivity of the combined spectrograph/camera system was sufficiently constant over the detected spectral range making a further correction unnecessary. Typically, ten emission spectra were recorded successively from one individual complex. In order to obtain a reasonable spectrally dispersed signal, we had to increase the excitation intensity to about 1 kW/cm^2. The integrity of the LH2 complexes was checked by recording the fluorescence−excitation spectra before and after the emission spectroscopy experiments for several LH2 complexes. Significant changes between the excitation spectra were not observable.

RESULTS AND DISCUSSION

In Figure 1 several examples of fluorescence−excitation (black lines) and emission spectra (colored lines) are shown that have been taken from the same individual LH2 complex. For comparison, the top traces show the respective ensemble spectra. As has been observed previously[13,54−57] the fluorescence−excitation spectra from individual complexes show remarkable differences which reflect the heterogeneity of the sample. Briefly, each complex and even each pigment within a complex experiences a slightly different local environment resulting in a slight change of the electrostatic interactions. This causes variations of the site energies of the BChl molecules as well as variations in the intermolecular interactions. In an ensemble of complexes this leads to an inhomogeneous broadening of the absorption line, which can be dismantled by studying the complexes individually. However, the excitation spectra have in common that they feature several narrow lines in the B800 spectral region and a few broad bands in the B850 region, reflecting the differences in lifetime/dephasing of the electronic states involved. Spectral variations are observed for the emission spectra as well. Yet to our surprise and in contrast to the excitation spectra the emission spectra can be grouped into three categories of qualitatively different spectra. In the first category (type I: 16 out of 44 complexes corresponding to 36%) the emission spectra show a relatively narrow spectral feature with a steep rise on the blue side and an asymmetric shoulder on the red side, Figure 1a. In the second category (type II: 22/44; 50%) the emission spectra show a broad featureless asymmetric band, Figure 1b. Finally in the third category (type III: 6/44; 14%) the emission spectra appear to be a superposition of the spectra found in the two other categories, Figure 1c.

Due to the low concentration of LH2 complexes the probability to find two LH2 complexes within the same excitation volume of 0.1 μm^3 is smaller than 0.01%, which

dx.doi.org/10.1021/jp3040456 | J. Phys. Chem. B 2012, 116, 11017−11023

makes it highly unlikely that all type III spectra result from two or more spatially unresolved LH2 complexes. Given the exposure time of 60 s for recording the emission spectra, it is more likely that this group of spectra stems from LH2 complexes that underwent a change in their emission characteristics during data acquisition. Therefore, for the detailed analysis that follows, we focus on the spectra in the first two categories.

Figure 2a shows examples of type I and type II emission spectra on an expanded scale.

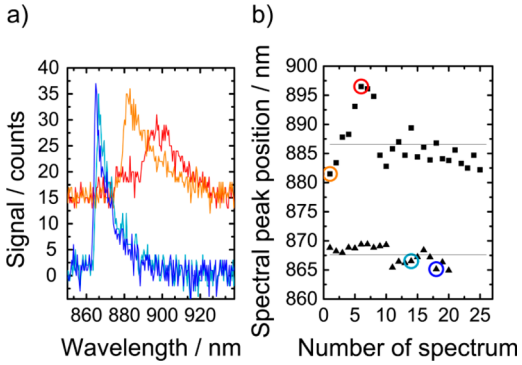

Figure 2. (a) Consecutively recorded type I (lower traces) and type II (upper traces) emission spectra. The time interval between the two examples selected for display was 240 s (type I) and 360 s (type II), respectively. The vertical axis is valid for the type I spectra, the type II spectra have been offset by 15 counts for clarity. (b) Spectral position of the peak of the emission spectrum as a function of exposures for type I (triangles) and type II (squares) spectra. The data have been recorded consecutively with an exposure time of 1 min per spectrum. The open circles correspond to the spectra shown in part a of the figure. The lines indicate the averaged peak positions.

Within each category the spectra have been recorded consecutively at a rate of one spectrum per minute from the same complex. Examples for the resulting spectra are shown in Figure 2a. The type I examples show only small changes between the two experiments. The spectral peaks occur at 866.5 and 865.0 nm, respectively, and the line width (fwhm) amounts to 133 and 125 cm^{-1}, respectively. In contrast, a drastic change with respect to both peak position (881.8 nm/898.9 nm) and line width (209 cm^{-1}/298 cm^{-1}) can be observed for the type II examples. Moreover, the shape of the spectrum changes from an asymmetric profile to a more symmetric one. For both complexes the changes in spectral peak position of the emission spectra as a function of the acquisitions are shown in Figure 2b. Although the type I spectrum shows only small peak shifts of less than ±3 nm (~40 cm^{-1}), much larger spectral excursions exceeding 10 nm (~130 cm^{-1}) were found for the type II spectra. Generally we found that the spectral stability was higher for type I as compared to type II spectra.

Furthermore, we found a clear trend that most of the type I spectra are blue-shifted with respect to the type II spectra.

This is clearly seen in Figure 3a, which displays the observed linewidths of the spectra as a function of the spectral peak position averaged over the observation time for all complexes studied, and which reveals a clear correlation between spectral position and line width/type of spectra. This is quantified in panels b and c in Figure 3 that show the distributions of the averaged peak positions, Figure 3b, and observed linewidths,

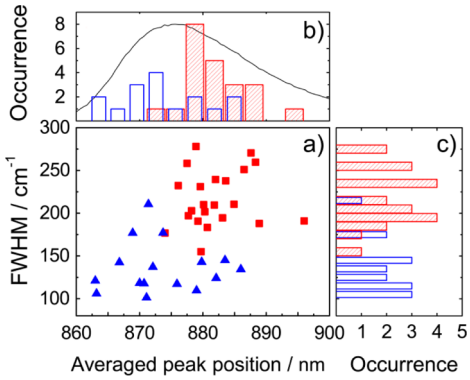

Figure 3. (a) Widths of the emission spectra as a function of the averaged peak position for type I (triangles) and type II (squares) spectra. (b) Distribution of the averaged peak positions for type I (blue) and type II (red) emission spectra. The overlaid black line corresponds to the emission spectrum from an ensemble of LH2 complexes. (c) Distribution of the widths for type I (blue) and type II (red) emission spectra.

Figure 3c, discriminated between type I (blue) and type II (red) spectra. The averaged peak positions of the emission spectra, Figure 3b, are distributed over the full spectral range that is covered by the ensemble emission spectrum (which has been overlaid (full line) for comparison). Yet the histogram for the type I spectra features a mean of 11 447 cm^{-1} (873.6 nm), which is clearly blue-shifted with respect to the mean value of 11 337 cm^{-1} (882.0 nm) that is found for the type II spectra. The mean of the line width distribution is 136 cm^{-1} for the type I spectra and 217 cm^{-1} for the type II spectra, see Figure 3c.

The striking differences in the spectral peak positions, spectral profiles, linewidths, and spectral diffusion behavior between the type I and type II emission spectra strongly suggests that there exist (at least temporarily) two pools of LH2 complexes that feature significant differences in their intra- and intermolecular interactions. For the type I emission spectra, we attribute the sharp spectral feature to the zero-phonon line (ZPL) and the asymmetric shoulder at higher wavelength to the phonon-sideband (PSB). The ZPL corresponds to the purely electronic transition, and the PSB corresponds to an electronic transition in combination with the simultaneous excitation of low-frequency vibrations. The distribution of the intensity between the ZPL and the PSB, is determined by the linear electron−phonon coupling strength. Information about this parameter can be obtained from the Debye−Waller factor, α, or likewise from the Huang−Rhys (HR) factor, S, which are given as

$$\alpha = \frac{I_{ZPL}}{I_{ZPL} + I_{PSB}} = \exp(-S) \quad (1)$$

Here I_{ZPL} and I_{PSB} refer to the integrated intensities of the ZPL and the PSB, respectively. The HR factor is a measure of the average number of phonons that accompany a particular electronic transition and can be associated with the displacement of the equilibrium positions of the nuclei upon a photoexcitation of the chromophore. In order to analyze the spectral profiles in more detail, we fitted the high-energy wing of the ZPL by a Lorentzian or Gaussian that was subtracted from the data to uncover the PSB as illustrated in Figure 4a.

Unfortunately, for some (mainly type II) spectra an unambiguous distinction between the ZPL and the PSB was

dx.doi.org/10.1021/jp3040456 | J. Phys. Chem. B 2012, 116, 11017−11023

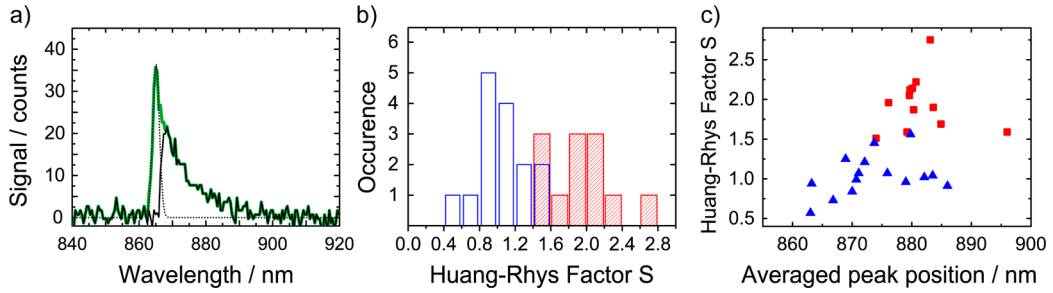

Figure 4. (a) Example of a type I emission spectrum (full green line). The low energy wing is fitted with a Gaussian (dotted line). The full black line corresponds to the difference spectrum between the signal and the fit function. (b) Histogram of the Huang–Rhys factors S for type I (blue) and type II (red) emission spectra. For the evaluation of the type II data, see text. (c) Huang–Rhys factors as a function of the averaged peak position of the emission spectrum for type I (triangles) and type II (squares) spectra.

impossible, and we therefore restrict the analysis to those spectra that allowed for a meaningful fitting of the ZPL (15 out of 16 for type I, and 12 out of 22 for type II). The resulting HR factors are shown in Figure 4b as a histogram, and in Figure 4c as a function of the averaged peak position of the emission spectrum. For type I spectra, Figure 4b blue bars, the HR factors covers the range from 0.6 - 1.6 peaking at 0.9. These numbers are slightly larger than those for the B800 BChl *a* molecules (0.2 - 0.9 peaking at 0.6)[58−61] and clearly larger than what has been found for BChl *a* in organic solvents (0.3 - 0.6).[62] For the type II spectra the HR factors cover the range from 1.5 - 2.8 with a mean around 2, Figure 4b red bars, which is in good agreement with the results obtained from fluorescence-line narrowing experiments by the Freiberg group.[28,63,64] From these data it can be stated that the type I spectra correlate with small HR factors; that is, there are no blue entries in the upper right corner of Figure 4c. However, we are not sensitive to type II complexes with a small HR factor which might be missed therefore.

Moreover the origin of the type II spectra is not as straightforward as suggested above. Next to reflecting a stronger exciton–phonon coupling, the broad and featureless profiles of the type II spectra could be the result of fast spectral diffusion processes, smearing out the typical ZPL/PSB profile. The two extremes are illustrated in Figure 5.

The top part of the figure displays schematically the configuration coordinate diagram for excitations in the B850 manifold. The potential curves of the electronic ground state and the lowest exciton states, denoted as $k = 0$ and $k = \pm 1$ are shown. For weak electron–phonon coupling, i.e., with no or only little horizontal displacement of the ground state and excited state potentials with respect to each other, the emission spectra feature a typical ZPL/PSB profile. Spectral diffusion (SD) corresponds to vertical displacements of the ground state and excited state potential energy curves with respect to each other. If these processes occur on time scales faster than the integration time of the CCD camera the typical ZPL/PSB profile is smeared out due to temporal averaging, see Figure 5 bottom left. This interpretation of the type II spectra is supported by the observation that such spectra in general show stronger spectral diffusion compared to type I spectra. Yet it does neither explain why the type I spectra are (predominantly) blue-shifted with respect to the type II spectra, nor does it explain the observed correlation between the spectral position and the HR factors for the type I spectra.

Alternatively, the type II spectra might reflect the formation of a self-trapped exciton state (STE). This is indicated in Figure 5 by the potential energy curve denoted STE. Emission from

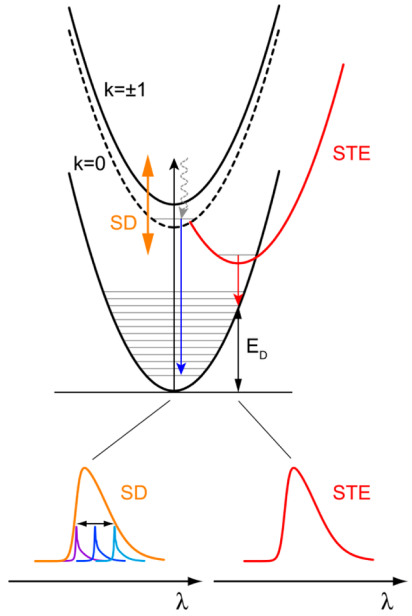

Figure 5. Configuration coordinate diagram of the electronic ground state (lowest potential energy curve) and the lowest exciton states ($k = 0$, dashed line, $k = \pm 1$ full line). For clarity the splitting between the $k = \pm 1$ states is neglected. Upon optical excitation (upward vertical arrow) the system relaxes to the lowest exciton state (wavy arrow). For weak electron phonon coupling the emission spectrum features a strong ZPL accompanied by a vibrational sideband (downward blue arrow, colored spectra bottom left). Spectral diffusion (SD) corresponds to vertical displacements of the potentials with respect to each other and is indicated by the double-headed arrow. If the spectral diffusion occurs on time scales faster than the data acquisition, temporal averaging smears out the spectral profile, and the measured spectrum corresponds to the envelope of the emission spectra, bottom left. For strong electron–phonon coupling the potential energy curves of the electronic ground state and the electronically excited states are horizontally shifted with respect to each other. This results in an emission spectrum with a strong vibrational sideband and only little or no intensity in the ZPL. Formation of a self-trapped exciton state (STE) lowers the potential energy with respect to the free exciton states ($k = 0$ and ± 1) reflected as an additional red shift of the spectrum, bottom right.

this state is significantly red-shifted and shows a broad featureless profile due to stronger electron–phonon coupling, Figure 5, bottom right, in line with the experimental findings. Moreover, this interpretation is supported by computer simulations for the self-trapped exciton model,[35,63] which predict progressively growing HR factors for decreasing

dx.doi.org/10.1021/jp3040456 | J. Phys. Chem. B 2012, 116, 11017–11023

emission energy that is in qualitative agreement with our experimental observations.

The formation of a self-trapped exciton is determined by the mutual time scales for the transfer of the excitation energy within the B850 assembly and the time that the nuclei need to react upon a change in the electronically excited state manifold.[40] This can be transformed into a coupling constant $g = E_D/\Delta$, where E_D corresponds to the lattice site deformation energy, and Δ denotes half of the exciton bandwidth.[38,41] A measure for E_D can be obtained from the separation between the ZPL and the spectral peak position of the PSB in the emission spectra, which is on the order of 50−100 cm^{-1}, and which differs from the energy E_D by the spatial extension of the self-trapped state; that is, the number of lattice sites over which the self-trapped exciton state is still delocalized. Hence, a typical lattice deformation energy E_D in the order of some 100 cm^{-1} is reasonable. Via the approximation $\Delta \approx 2V$ the half-width of the exciton band can be obtained from the intermolecular interaction strength, V, for which several estimates exist in the literature, covering the range between 250 and 400 cm^{-1}.[56,65] From these figures we obtain $g \approx E_D/2V$ that is on the order of 0.1−0.5 and is in quantitative agreement with the numerical values used for the simulations detailed in refs 35 and 63.

Although we cannot exclude spectral diffusion as the origin of some of the type II emission spectra, the current results together with the results from other experimental techniques[20,41−43] and from the simulations in refs 35 and 63 strongly suggest that for a part of the complexes that feature type II emission spectra exciton self-trapping does take place. This interpretation explains straightforwardly the discrepancies that have been found between the absorption and emission spectra as mentioned in the introduction. Due to self-trapping of the exciton, the absorbing state and the emitting state are not equivalent. Therefore, conclusions drawn from experiments that monitor properties of the absorbing state do not necessarily agree with conclusions drawn from experiments that monitor the properties of the emitting state. This is in line with the observation that the widths of the hole-burning action spectra of the lowest exciton state[19−21,28,63] and the ensemble emission spectra do not match and why in single-molecule spectroscopy the remarkable differences between type I and type II emission spectra are not reflected in the fluorescence−excitation spectra. Another discrepancy concerns the exciton delocalization length. Fluorescence−excitation spectroscopy monitors transitions from the electronic ground state to the electronically excited state; that is, it monitors the exciton state when it is "born". In contrast, time-resolved spectroscopy monitors the reverse transition corresponding to the decay or "death" of the exciton. Therefore it refers to the delocalization of the exciton after relaxation (and STE formation) in the excited state manifold. According to[38] the number of units on which the STE is localized is given by $N \approx 1/2g$, which yields for the estimate given above $N \approx 1-5$. Interestingly, these numbers agree with what has been found by time-resolved spectroscopy.[20,31−34] Yet, it is reasonable to assume that for a distinct LH2 complex the coupling parameter g, which determines the formation of a self-trapped exciton state, has not a fixed value but rather fluctuates in time. In the illustration shown in Figure 5 this corresponds to a temporal variation of the position of the STE state (red parabola) along both the vertical and the horizontal direction. Whether this is of relevance for the biological function, for example for enhancing the energy transfer between adjacent LH2 complexes, remains an open question at this point.

CONCLUSIONS

Low temperature fluorescence−excitation and emission spectroscopy has been performed on individual LH2 complexes from *Rps. acidophila*. According to their shape the emission spectra can be grouped in two categories. One category features a narrow spectral profile containing a zero-phonon line, whereas the spectra of the other type display broad featureless bands. For each group of spectra, clear correlations between the spectral positions, the widths of the spectral profiles, and the electron−phonon coupling strength have been found. Interestingly the differences in the emission spectra between individual LH2 complexes are not reflected in their corresponding fluorescence−excitation spectra. Although fast unresolved spectral diffusion cannot be fully ruled out as being the origin for the broad spectra, the observed correlations lead us to conclude that at least for some of the LH2 complexes an exciton self-trapping process is effective.

AUTHOR INFORMATION

Corresponding Author

*Telephone: +49 921 55 4000. Fax: +49 921 55 4002. E-mail: juergen.koehler@uni-bayreuth.de.

Notes

The authors declare no competing financial interest.

ACKNOWLEDGMENTS

We gratefully acknowledge financial support from the Deutsche Forschungsgemeinschaft (KO 1359/16-1, GZ: 436 EST 113/4/0-1 and GRK1640). A.F. and K.T. are also partially supported by the Estonian Science Foundation (Grant No. 8674) and the Ministry of Education and Science (Grant SF0180055s07).

ABBREVIATIONS

BChl: bacteriochlorophyll; LH1: light harvesting 1 (complex); LH2: light harvesting 2 (complex); RC: reaction center

REFERENCES

(1) McDermott, G.; Prince, S. M.; Freer, A. A.; Hawthornthwaite-Lawless, A. M.; Papiz, M. Z.; Cogdell, R. J.; Isaacs, N. W. *Nature* **1995**, *374*, 517−521.

(2) McLuskey, K.; Prince, S. M.; Cogdell, R. J.; Isaacs, N. W. *Biochemistry* **2001**, *40*, 8783−8789.

(3) Koepke, J.; Hu, X.; Muenke, C.; Schulten, K.; Michel, H. *Structure* **1996**, *4*, 581−597.

(4) Roszak, A. W.; Howard, T. D.; Southall, J.; Gardiner, A. T.; Law, C. J.; Isaacs, N. W.; Cogdell, R. J. *Science* **2003**, *302*, 1969−1971.

(5) Qian, P.; Neil Hunter, C.; Bullough, P. A. *J. Mol. Biol.* **2005**, *349*, 948−960.

(6) Cogdell, R. J.; Gardiner, A. T.; Roszak, A. W.; Law, C. J.; Southall, J.; Isaacs, N. W. *Photosynth. Res.* **2004**, *81*, 207−214.

(7) Davydov, A. S. *Theory of Molecular Excitons*; Plenum Press: New York, 1971.

(8) Knox, R. S. *Theory of Excitons*; Ehrenreich, H., Seitz, F., Turnbull, D., Eds.; Academic Press: New York, 1963; pp 7−37.

(9) Robinson, C. W. *Annu. Rev. Phys. Chem.* **1970**, *21*, 429−474.

(10) Wu, H.-M.; Rätsep, M.; Lee, I.-J.; Cogdell, R. J.; Small, G. J. *J. Phys. Chem. B* **1997**, *101*, 7654−7663.

(11) Alden, R. G.; Johnson, E.; Nagarajan, V.; Parson, W. W.; Law, C. J.; Cogdell, R. J. *J. Phys. Chem. B* **1997**, *101*, 4667−4680.

(12) van Oijen, A. M.; Ketelaars, M.; Köhler, J.; Aartsma, T. J.; Schmidt, J. *Science* **1999**, *285*, 400−402.
(13) Ketelaars, M.; van Oijen, A. M.; Matsushita, M.; Köhler, J.; Schmidt, J.; Aartsma, T. J. *Biophys. J.* **2001**, *80*, 1591−1603.
(14) Matsushita, M.; Ketelaars, M.; van Oijen, A. M.; Köhler, J.; Aartsma, T. J.; Schmidt, J. *Biophys. J.* **2001**, *80*, 1604−1614.
(15) Mostovoy, M. V.; Knoester, J. *J. Phys. Chem. B* **2000**, *104*, 12355−12364.
(16) Jang, S.; Silbey, R. J. *J. Chem. Phys.* **2003**, *118*, 9324−9336.
(17) Jang, S.; Silbey, R. J.; Kunz, R.; Hofmann, C.; Köhler, J. *J. Phys. Chem. B* **2011**, *115*, 12355−12953.
(18) Hofmann, C.; Aartsma, T. J.; Köhler, J. *Chem. Phys. Lett.* **2004**, *395*, 373−378.
(19) Timpmann, K.; Katiliene, Z.; Woodbury, N. W.; Freiberg, A. *J. Phys. Chem. B* **2001**, *105*, 12223−12225.
(20) Freiberg, A.; Rätsep, M.; Timpmann, K.; Trinkunas, G.; Woodbury, W. N. *J. Phys. Chem. B* **2003**, *107*, 11510−11519.
(21) Wu, H.-M.; Reddy, N. R. S.; Small, G. J. *J. Phys. Chem. B* **1997**, *101*, 651−656.
(22) Rätsep, M.; Hunter, C. N.; Olsen, J. D.; Freiberg, A. *Photosynth. Res.* **2005**, *86*, 37−48.
(23) Richter, M. F.; Baier, J.; Prem, T.; Oellerich, S.; Francia, F.; Venturoli, G.; Oesterhelt, D.; Southall, J.; Cogdell, R. J.; Köhler, J. *Proc. Natl. Acad. Sci. U.S.A.* **2007**, *104*, 6661−6665.
(24) Creemers, T. M. H.; de Caro, C.; Visschers, R. W.; van Grondelle, R.; Völker, S. *J. Phys. Chem. B* **1999**, *103*, 9770−9776.
(25) Reddy, N. R.; Picorel, R.; Small, G. J. *J. Phys. Chem.* **1992**, *96*, 6458−6464.
(26) van Mourik, F.; Visschers, R. W.; van Grondelle, R. *Chem. Phys. Lett.* **1992**, *193*, 1−7.
(27) Monshouwer, R.; Visschers, R. W.; van Mourik, F.; Freiberg, A.; van Grondelle, R. *Biochim. Biophys. Acta, Bioenerg.* **1995**, *1229*, 373−380.
(28) Timpmann, K.; Rätsep, M.; Hunter, C. N.; Freiberg, A. *J. Phys. Chem. B* **2004**, *108*, 10581−10588.
(29) Ketelaars, M.; Hofmann, C.; Köhler, J.; Howard, T. D.; Cogdell, R. J.; Schmidt, J.; Aartsma, T. J. *Biophys. J.* **2002**, *83*, 1701−1715.
(30) Richter, M. F.; Baier, J.; Southall, J.; Cogdell, R. J.; Oellerich, S.; Köhler, J. *Proc. Natl. Acad. Sci. U.S.A.* **2007**, *104*, 20280−20284.
(31) Pullerits, T.; Chachisvillis, M.; Sundström, V. *J. Phys. Chem.* **1996**, *100*, 10787−10792.
(32) Novoderezhkin, V. I.; Monshouwer, R.; van Grondelle, R. *J. Phys. Chem. B* **1999**, *103*, 10540−10548.
(33) Freiberg, A.; Timpmann, K.; Lin, S.; Woodbury, N. W. *J. Phys. Chem. B* **1998**, *102*, 10974−10982.
(34) Trinkunas, G.; Freiberg, A. *J. Lumin.* **2006**, *119−120*, 105−110.
(35) Freiberg, A.; Trinkunas, G. *Photosynthesis in Silico: Understanding Complexity From Molecules to Ecosystems*; Laisk, A., Nedbal, L., Govindjee, Eds.; Springer: Netherlands, 2009; Vol. *29*, pp 55−82.
(36) Toyozawa, Y. *Prog. Theor. Phys.* **1958**, *20*, 53−81.
(37) Rashba, E. I. *Excitons*; Rashba, E. I., Sturge, M. D., Eds.; North-Holland Publishing Company: North-Holland, 1982; Vol. *2*, pp 544−602.
(38) Sumi, H.; Sumi, A. *J. Phys. Soc. Jpn.* **1994**, *63*, 637−657.
(39) Toyozawa, Y. *Optical Processes in Solids*; Toyozawa, Y., Ed.; Cambridge University Press: Cambridge, 2003; pp 149−191.
(40) Knoester, J.; Agranovich, V. M. *Thin Films and Nanostructures*: Elsevier: Amsterdam, 2003; Vol. *31*, pp 1−96.
(41) Freiberg, A.; Rätsep, M.; Timpmann, K.; Trinkunas, G. *J. Lumin.* **2003**, *102−103*, 363−368.
(42) Trinkunas, G.; Freiberg, A. *J. Lumin.* **2005**, *112*, 420−423.
(43) Pajusalu, M.; Rätsep, M.; Trinkunas, G.; Freiberg, A. *ChemPhysChem* **2011**, *12*, 634−644.
(44) Bopp, M. A.; Sytnik, A.; Howard, T. D.; Cogdell, R. J.; Hochstrasser, R. M. *Proc. Natl. Acad. Sci. U.S.A.* **1999**, *96*, 11271−11276.
(45) Tietz, C.; Cheklov, O.; Dräbenstedt, A.; Schuster, J.; Wrachtrup, J. *J. Phys. Chem. B* **1999**, *103*, 6328−6333.
(46) Gerken, U.; Jelezko, F.; Götze, B.; Branschädel, M.; Tietz, C.; Ghosh, R.; Wrachtrup, J. *J. Phys. Chem. B* **2003**, *107*, 338−343.
(47) Gerken, U.; Lupo, D.; Tietz, C.; Wrachtrup, J.; Ghosh, R. *Biochemistry* **2003**, *42*, 10354−10360.
(48) de Ruijter, W. P. F.; Segura, J. M.; Cogdell, R. J.; Gardiner, A. T.; Oellerich, S.; Aartsma, T. J. *Chem. Phys.* **2007**, *341*, 320−325.
(49) Novoderezhkin, V. I.; Rutkauskas, D.; van Grondelle, R. *Chem. Phys.* **2007**, *341*, 45−56.
(50) Uchiyama, D.; Oikawa, H.; Otomo, K.; Nango, M.; Dewa, T.; Fujiyoshi, S.; Matsushita, M. *Phys. Chem. Chem. Phys.* **2011**, *13*, 11615−11619.
(51) Tubasum, S.; Thomsson, D.; Cogdell, R.; Scheblykin, I.; Pullerits, T. *Photosynth. Res.* **2011**, *111*, 41−45.
(52) Hofmann, C.; Kulzer, F.; Zondervan, R.; Köhler, J.; Orrit, M. *Single Molecules and Nanotechnology*; Rigler, R., Vogel, H., Eds.; Springer: Heidelberg, 2008; Vol. *12*, pp 25−51.
(53) Cogdell, R.; Hawthornthwaite, A. M. *The Photosynthetic Reaction Center*; Deisenhofer, J., Norris, J. R., Eds.; Academic Press: San Diego, CA, 1993; Vol. *1*, pp 23−42.
(54) Hofmann, C.; Francia, F.; Venturoli, G.; Oesterhelt, D.; Köhler, J. *FEBS Lett.* **2003**, *546*, 345−348.
(55) Brotosudarmo, T. H. P.; Kunz, R.; Böhm, P.; Gardiner, A. T.; Moulisová, V.; Cogdell, R. J.; Köhler, J. *Biophys. J.* **2009**, *97*, 1491−1500.
(56) Cogdell, R. J.; Gall, A.; Köhler, J. *Q. Rev. Biophys.* **2006**, *39*, 227−324.
(57) Berlin, Y.; Burin, A.; Friedrich, J.; Köhler, J. *Phys. Life Rev.* **2007**, *4*, 64−89.
(58) Wu, H.-M.; Savikhin, S.; Reddy, N. R. S.; Jankowiak, R.; Cogdell, R. J.; Struve, W. S.; Small, G. J. *J. Phys. Chem.* **1996**, *100*, 12022−12033.
(59) Small, G. J. *Chem. Phys.* **1995**, *197*, 239−257.
(60) Hofmann, C.; Michel, H.; van Heel, M.; Köhler, J. *Phys. Rev. Lett.* **2005**, *94*, 195501.
(61) Baier, J.; Gabrielsen, M.; Oellerich, S.; Michel, H.; van Heel, M.; Cogdell, R. J.; Köhler, J. *Biophys. J.* **2009**, *97*, 2604−2612.
(62) Rätsep, M.; Cai, Z.-L.; Reimers, J. R.; Freiberg, A. *J. Chem. Phys.* **2011**, *134* (024506), 1−15.
(63) Freiberg, A.; Rätsep, M.; Timpmann, K.; Trinkunas, G. *Chem. Phys.* **2009**, *357*, 102−112.
(64) Rätsep, M.; Freiberg, A. *Chem. Phys. Lett.* **2003**, *377*, 371−376.
(65) Freiberg, A.; Timpmann, K.; Trinkunas, G. *Chem. Phys. Lett.* **2010**, *500*, 111−115.